ACS OMEGA

http://pubs.acs.org/journal/acsodf

Article

Chitosan-Coated Niosomes Loaded with Ellagic Acid Present Antiaging Activity in a Skin Cell Line

Amr A. Abd-Elghany* and Ebtesam A. Mohamad

Cite This: *ACS Omega* 2023, 8, 16620−16629

Read Online

ACCESS | Metrics & More | Article Recommendations

ABSTRACT: The polyphenol compound ellagic acid (EA) extracted from pomegranate has potential bioactivity against different types of chronic diseases. Skin aging is a long-term physiological process caused by many environmental factors, the most important of which is exposure to sun ultraviolet (UV) radiation. UV-induced chronic photodamage of the skin results in extrinsic aging. This study aimed to evaluate the photoprotective effects of EA on the human fibroblast skin cell line HFB4 and investigate its capacity to protect collagen from UV-induced deterioration. EA was encapsulated into chitosan-coated niosomes to reduce the skin aging effect of UV radiation in vitro. The tested formulations (niosomes loaded with EA and chitosan-coated niosomes loaded with EA) were characterized using transmission electron microscopy, dynamic light scattering, and scanning electron microscopy. Furthermore, the in vitro release of EA was determined. The HFB4 cell line samples were split into five groups: control, UV, UV-EA, UV-NIO-EA, and UV-CS-NIO-EA. UV irradiation was applied to the cell line groups via a UV-emitting lamp for 1 h, and then cell viability was measured for each group. The expression of genes implicated in skin aging (Co1A1, TERT, Timp3, and MMP3) was also assessed to quantify the impact of the loaded EA. The findings showed that EA-loaded chitosan-coated niosomes improved cell survival, upregulated Col1A1, TERT, and Timp3 genes, and downregulated MMP3. Thus, nanoparticles encapsulating EA are potent antioxidants that can preserve collagen levels and slow down the aging process in human skin.

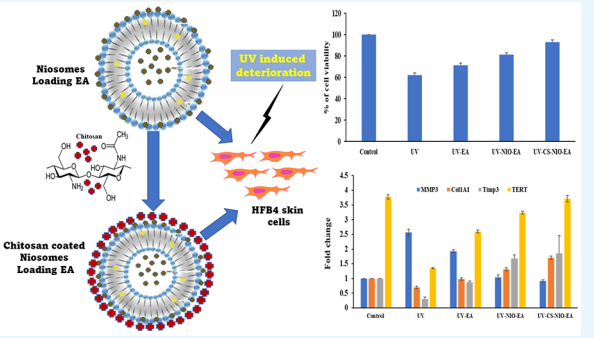

1. INTRODUCTION

The population of adults aged 60 years or older is increasing worldwide, which may influence the morbidity and mortality of skin diseases as well as the organization of the healthcare systems. Except for Africa, all regions of the world, especially high-income countries, will have at least a quarter of their population aged 60 or over by 2050.[1] The aging process of the skin begins from the moment of birth, which is unique and relative to other body systems that reach maturity at a more advanced stage of life.[2] The problem of skin aging is significant and a cause for concern, particularly among women. A large amount of money is spent annually to counteract the skin aging process.[3,4] Dermatological research strategies for addressing this problem are focused on identifying natural low-cost plant extracts that have no or minimum side effects.[5−7] Natural plant extracts are rich in antioxidants and at the same time can absorb ultraviolet rays, which is the main cause of skin aging.[5,8]

Ultraviolet (UV) light is considered one of the main causes of DNA damage, inflammation, and various skin lesions such as those from photocarcinogenesis and photoaging.[9−11] Most of the usual histological and clinical signs of chronic photodamage of the skin are complications of DNA photodamage and UV-induced reactive oxygen species (ROS), which are the earliest molecular events.[12] UVA radiation (UVA; 320−400 nm) represents from 95 to 98% of all UV photons that hit Earth's surface. UVA rays not only harm the epidermis but also tear down collagen and elastin deep within the dermis.[13] ROS, which are created by UV irradiation, control a wide range of biological processes, including collagen breakdown and MMP production.[14]

Collagen is a structural protein found in many body parts and accounts for between 25 and 35% of the body's total protein content, making it the most prevalent protein in humans. Collagen production is controlled by members of the collagen gene family, including *COL1A1*.[15] It is found in the extracellular matrix (ECM) of the dermal layer of the skin to provide it with strength and elasticity, which makes the skin more youthful and vibrant.[16,17] Skin wrinkles, a sign of photoaging, are caused by the deterioration of ECM integrity in the skin. Aged skin extensively expresses the matrix metalloproteinase (*MMP*3)

Received: November 11, 2022
Revised: March 18, 2023
Accepted: April 26, 2023
Published: May 3, 2023

gene, which disrupts the ECM.[18] Fibrillar collagen and elastin, which contribute to skin strength and elasticity, are attacked by collagenolytic MMP enzymes.[19] Previous studies have also shown the significance of tissue inhibitor metalloproteinase genes, such as *TIMP*3, which are crucial in preventing the breakdown of ECM's proteins.[20] Other genes also play a role in skin aging, such as telomerase reverse transcriptase (*TERT*).[10] Telomeres are located at the ends of chromosomes, and their function, which is like that of the metal clip at the end of a shoelace, is to keep the chromosome and genetic material intact without destruction or synapsis with the surrounding chromosomes. The telomere shortens after each cell division until it becomes too short to allow for further cell divisions, and cell aging subsequently occurs.[21]

Ellagic acid (EA) is a polyphenolic compound found in some types of fruit, such as strawberries, blueberries, and pomegranates.[22] Pomegranate fruit extract (PFE) shows antioxidative activity caused by the action of EA.[23] Research findings show that EA is a potential biomolecule with remarkable biological features, such as UV shielding and anticancer functionalities.[24−26] It is also a potent antioxidant and antibacterial agent.[27,28] EA is made up of four hydroxyl groups and several lactone rings, which are hydrophilic.[29] However, its low bioavailability limits its therapeutic effect.[30] Nanotechnology can overcome the limitations of EA by encapsulating EA into biocompatible carriers. Niosomes have a similar structure to liposomes since they are a type of carrier system that encapsulates drugs in vesicles with a bilayer structure made of nonionic surfactants like polysorbate 80 (Tween 80) and stabilized with cholesterol.[31,32] The hydrophilic heads of polysorbate 80 are polyethers, commonly known as polyoxyethylene groups, which are ethylene oxide polymers. The lipophilic tails of Tween 80 are composed of oleic acid.[33] Tween 80 functions as a P-glycoprotein inhibitor. It has been observed that nanoparticles based on Tween 80 can block P-glycoprotein-mediated drug exocytosis.[29] The amphiphilic bilayer structure and poor water solubility of niosomes promote drug bioavailability by trapping the drug inside the structure and allowing penetration of biological membranes, hence improving therapeutic effectiveness. Unlike liposomes, niosomes have improved physicochemical stability and drug retention in vitro and in vivo.[32,34,35] This could further be complemented with chitosan, which is an effective drug-delivery polymer that protects the drugs from degradation, thereby promoting drug sustainability and enabling drugs to reach the target site.[36] This study tests the antiaging activity of EA carried by chitosan-coated niosomes in the human fibroblast cell line HFB4 in which UV photodamage was induced.

2. RESULTS AND DISCUSSION

In the current study, a biomaterial nanocarrier system was designed by encapsulating EA into niosome nanoparticles covered by a chitosan layer.

2.1. Encapsulation Efficiency (EE) and Morphology of Niosomes. The encapsulation efficiency (EE) % values of EA in NIO-EA NPs and CS-NIO-EA NPs were 60 ± 4 and 74 ± 3.1%, respectively. There was a significant difference in the recorded EE % in NIO-EA and Cs-NIO-EA NPs. EA is a hydrophilic drug, which was attached to the heads of the niosomal vesicles probably through adhesive force. EA molecules are hydrophilic, so they were attached to the outer shell of the niosomes and inside, and the centrifugation process causes the loss of surface-bound EA molecules in the case of NIO-EA NPs, while in Cs-NIO-EA NPs, the process of coating the niosomes with chitosan and encapsulating it with EA takes place simultaneously, allowing the rigid layer of chitosan to protect EA molecules attached to the surface, which increase EE % in Cs-NIO-EA NPs. Another possible reason was that Cs-NIO-EA NPs may be coated by an extra chitosan layer causing them to entrap more EA molecules. The same results were obtained previously by coating niosomes with a surfactant.[29] The entrapment efficiency was not higher due to the use of Tween 80. Tween 80 is composed of a chain of unsaturated alkyls. The presence of double bonds caused the chains to bend, resulting in the creation of an inadequately tight niosomal membrane. Therefore, the membrane of the niosomes was more permeable, which may account for the reduced entrapment effectiveness of the Tween 80 formulations.[37] Additionally, a report has indicated that the entrapment efficiency was increased by increasing the cholesterol content, which was less than 50% of the total surfactant content in our study. Cholesterol can increase the hydrophobicity of the bilayer, which reduces the surface free energy and, in turn, reduces the particle size and improves the entrapment efficiency.[38] The present finding is consistent with that of a previous study.[39] The results of a transmission electron microscopy (TEM) morphological analysis of the NIO-EA NPs and CS-NIO-EA are shown in Figure 1a,b. The images of the

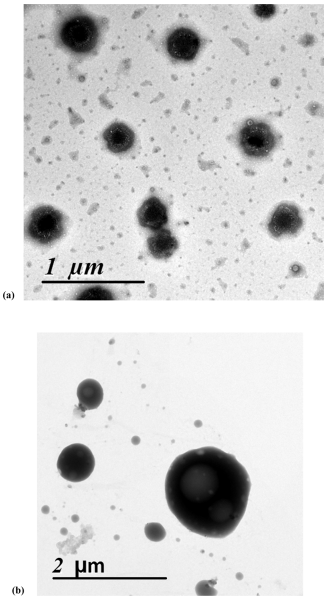

Figure 1. TEM images: NIO-EA NPs (a) and CS-NIO-EA NPs (b).

nanoparticles showed nonaggregated and spherical-like particles (Figure 1a). A previous study postulated that chitosan can be arranged on the outer vesicular surface forming a three-dimensional shell after cross-linking with tripolyphosphate.[40] In the present study, the niosomal size was increased by 2.63 times after coating the niosomes with chitosan (Figure 1b). The chitosan coating around the NIO-EA NPs is shown in Figure 1b as a smooth chitosan shell, and the size of the particles increased because of the presence of the chitosan coat around the loaded niosomes. Because of the extremely dense matrix incorporated into the nanoparticles, the particles' inner black hue could be observed. The fractions with low radii observed in both images were of the same nature as macromolecules. This diversity in sizes was attributed to the difficulty of standardizing all sizes, and

https://doi.org/10.1021/acsomega.2c07254
ACS Omega 2023, 8, 16620−16629

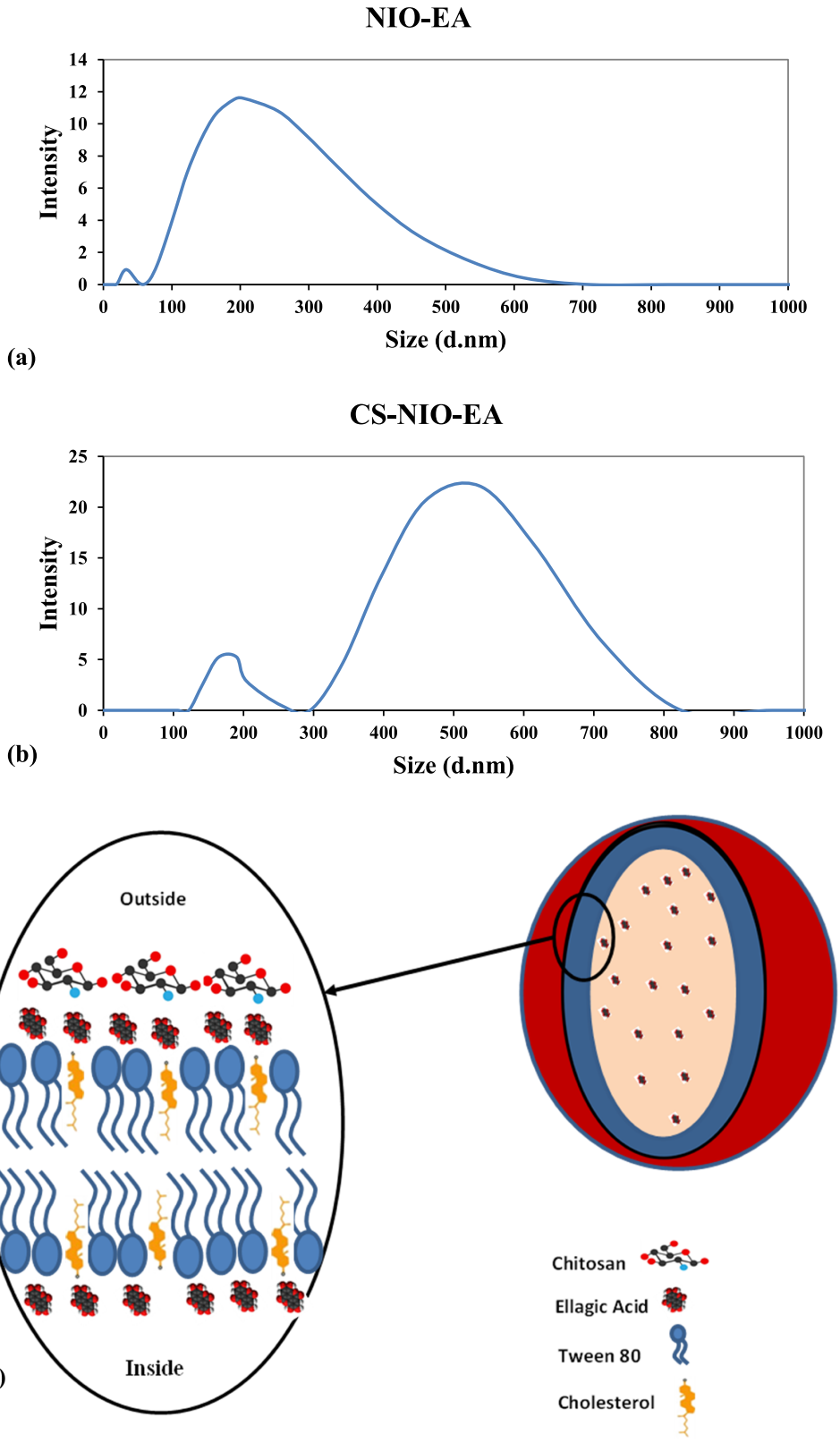

Figure 2. Average particle size of NIO-EA (PDI = 0.134) (a) CS-NIO-EA (PDI = 0.87). (b) and (c) Illustration of intermolecular interactions.

they were subjected to sonication, and they began to crack randomly.

2.2. Size Distribution. Particle size is a characteristic parameter for nanoparticles. The length of the alkyl chain in surfactants affects the size of niosomes.[41] Dynamic light scattering (DLS) was used to measure the size of NIO-EA and CS-NIO-EA NPs. The NIO-EA NPs had a particle size of 204 ± 7.2 nm, whereas the chitosan-coated NIO-EAs (CS-NIO-EAs) were larger at 536.7 ± 131.6 nm (Figure 2a,b). The polydispersity index (PDI) increased from 0.134 for NIO-EA

https://doi.org/10.1021/acsomega.2c07254
ACS Omega 2023, 8, 16620−16629

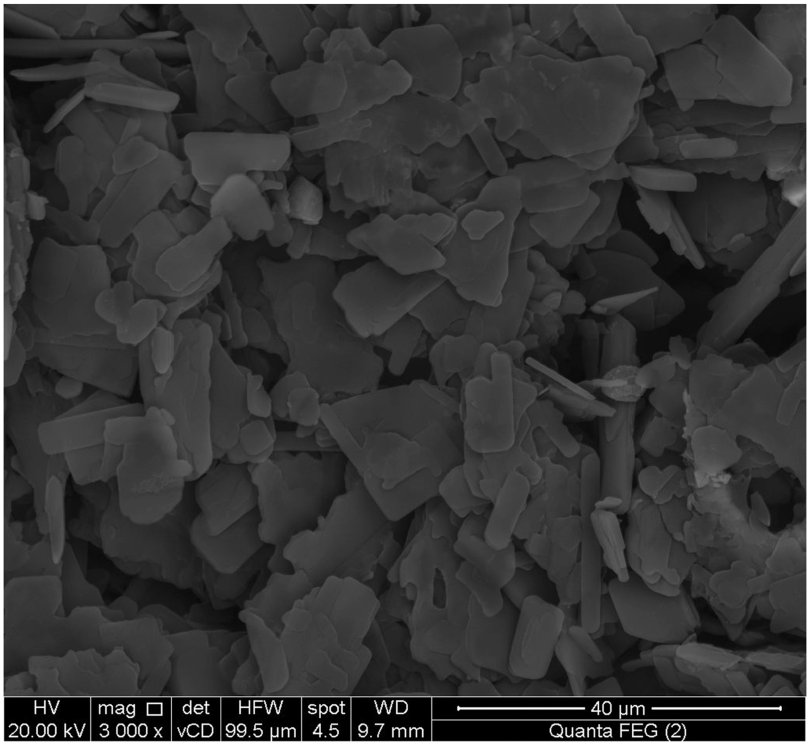

(a)

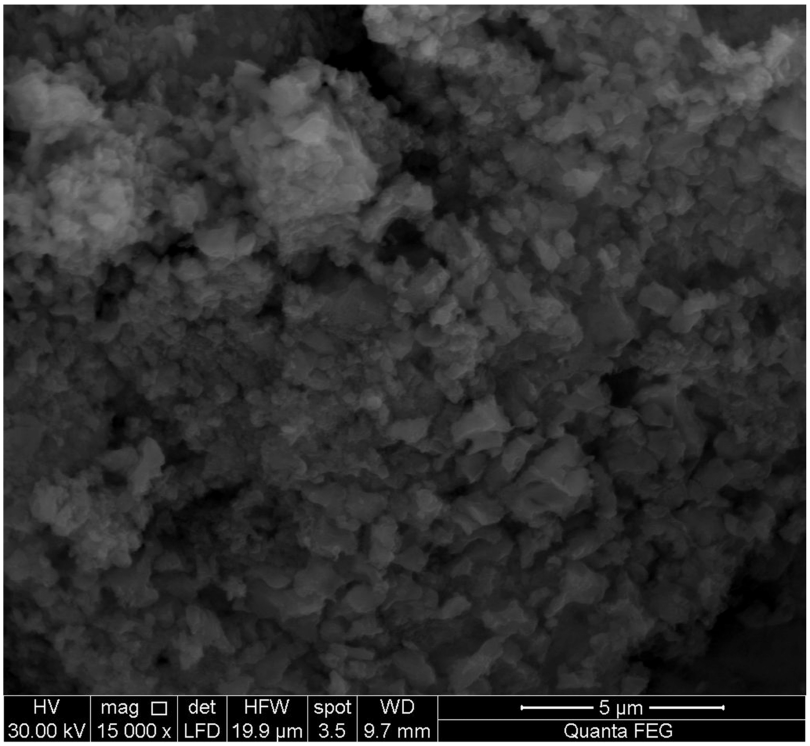

(b)

Figure 3. SEM images: NIO-EA NPs (a) and CS/NIO-EA NPs (b).

to 0.87 for CS-NIO-EA. The hydrophilic EA molecules could be bound on the outer shell of niosomes by adhesive forces with the hydrophilic heads of Tween 80. The chitosan coat around the niosomes loaded with EA increased the size of the nanoparticles due to the formation of a hydrophilic envelope on the surface by ionic interaction.[35] This interaction is due to the interaction between the reactive negatively charged hydroxyl groups of EA and the positively charged amino group in chitosan.[42] In addition, strong hydrogen bonds were formed between the hydroxyl group of EA and the amino groups present in the chitosan.[43,44] The arrangement of Cs, EA, Tween 80, and cholesterol is illustrated in Figure 2c.

https://doi.org/10.1021/acsomega.2c07254
ACS Omega 2023, 8, 16620−16629

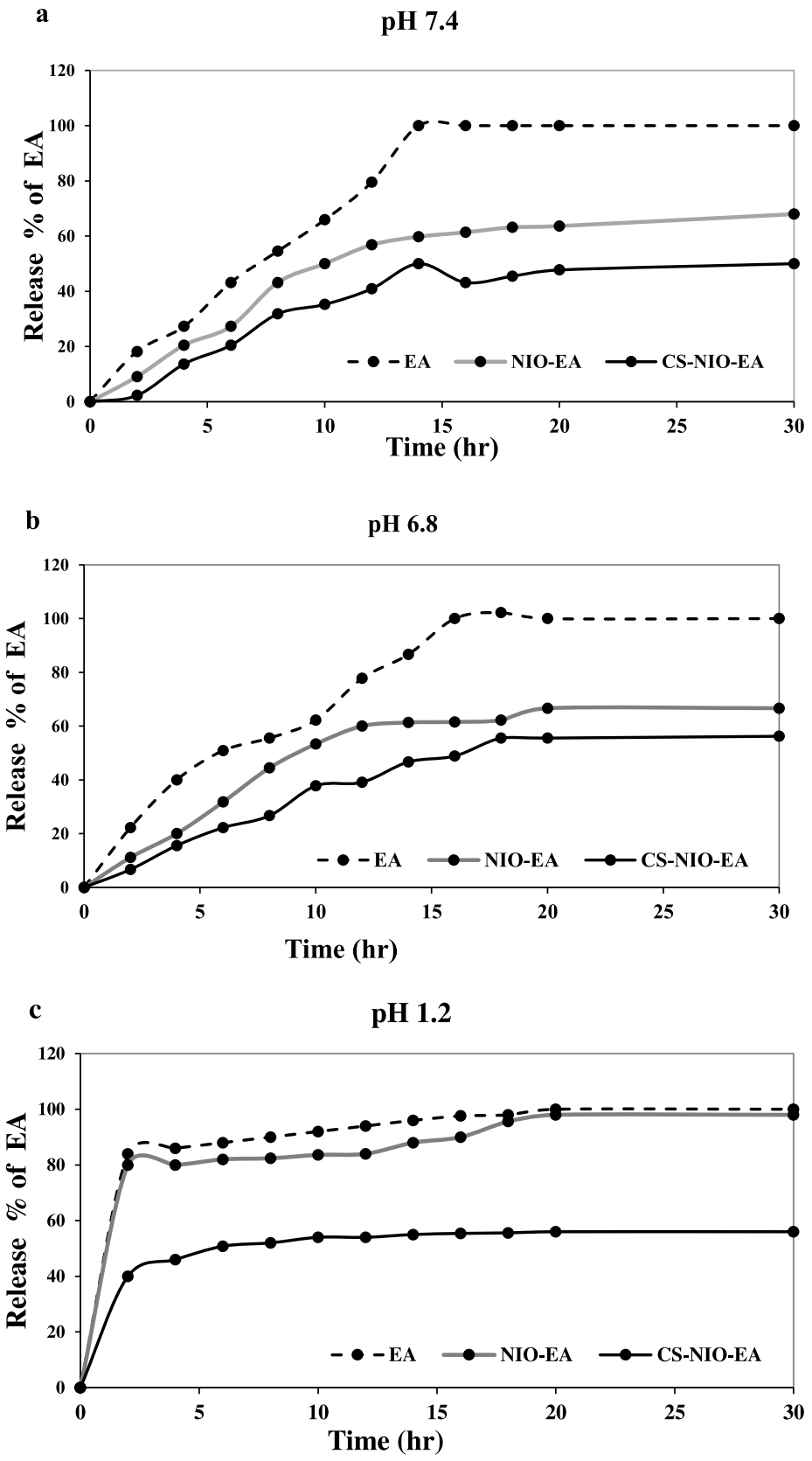

Figure 4. In vitro release profiles of free EA, NIO-EA NPs, and CS-NIO-EA NPs at pH values 7.4 (a), 6.8 (b), and 1.2 (c).

This increase in particle size enhances the efficacy of CS-NIO-EA in terms of drug encapsulation and release. It has been estimated that chitosan enhances the drug transport through cell membranes and cellular pathways.[45] The ζ-potentials of NIO-EA and CS-NIO-EA were -5.95 ± 0.98 and -30 ± 2.23 mV, respectively.

2.3. Surface Morphology Analysis. The surface morphologies of the lyophilized samples were examined by scanning

https://doi.org/10.1021/acsomega.2c07254
ACS Omega 2023, 8, 16620−16629

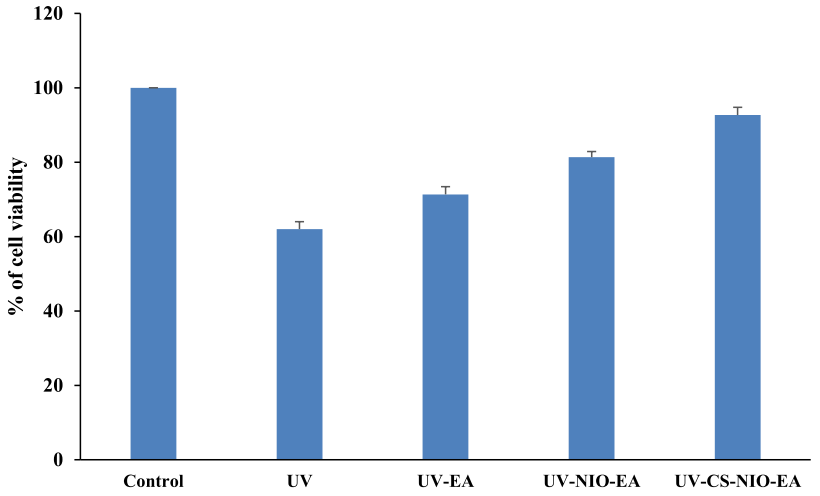

Figure 5. Effect of the different treatments on the percentage of cell viability.

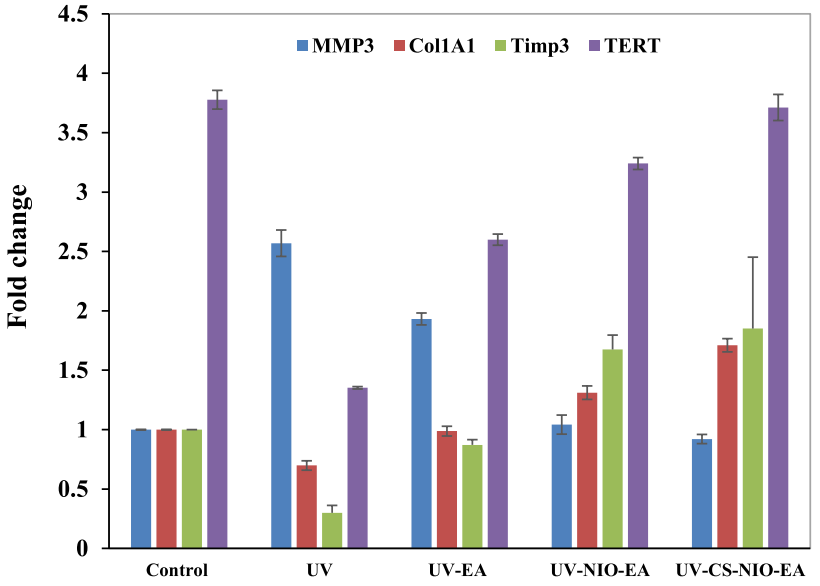

Figure 6. Fold change of Col1A1, Timp3, TERT, and MMP3 gene expressions in the five groups. The error bars represent standard deviations (SDs).

electron microscope (SEM). The resulting NIO-EA NP samples appeared in the form of plates with smooth surface and different sizes (Figure 3a) because of the preparation method that relies on compressing the surface of the samples that have been converted into powder by freeze drying. The drying process may explain the plate irregularities that were noticed during the investigation.[41] Upon the incorporation of chitosan (CS-NIO-EA NPs), the surface roughness increased (Figure 3b), and the spheroidal vesicles decreased. The results were confirmed by previous studies.[46−48] In addition, the chitosan coating layer of the CS-NIO-EA NPs could further improve the physical stability of the NPs[35] because it provided rigidity to the bilayer membrane and reduced the fluidity of the bilayer by removing the phase transition temperature peak of the vesicles.[49]

2.4. In Vitro Release Profile of Free and Encapsulated EAs. Nanotechnology aims to identify excellent drug encapsulations to achieve a desirable controllable release profile for a specific drug. For medication that is administrated orally, three different pH media were used to evaluate the release of EA from the niosomal formulations. In vitro release was used to study the release of the prepared formulations. Figure 4a−c shows the cumulative release profiles of EA before and after encapsulation into the prepared nanocarriers over a period of 30 h. The cumulative release of the investigated formulations was compared with the free EA release profile, which was considered as the control release.

The cumulative release profiles of NIO-EA NPs showed that the amount of EA released after 8 h was 43.18% on phosphate-buffered saline (PBS) pH 7.4, 44.44% on PBS pH 6.8, and 82.4% on 0.1 N HCl pH 1.2 media, whereas that of CS-NIO-EA NPs showed that the amount of EA released was 31.82% on PBS pH 7.4, 26.67% on PBS pH 6.8, and 52% on 0.1 N HCl pH 1.2 media. Thus, the chitosan coating decreased the amount of the EA released compared to that of the NIO-EA NPs for all pH media. After 14 h, the CS-NIO-EA NP profile reached the saturated release plateau of EA, with values of 50, 46.67, and 55% observed for pH values 7.4, 6.8, and 1.2 media, respectively. The saturated release profile has been confirmed by other studies.[35,49]

The pH of the surrounding media affects EA's capacity to scavenge free radicals.[50] EA may be ionized partially or completely. Deprotonation can occur in all four phenolic

https://doi.org/10.1021/acsomega.2c07254
ACS Omega 2023, 8, 16620−16629

groups, which would imply four pK_a values. However, the symmetric phenolic substituents in EA typically have two pK_a values attributed to them: 4-/4′-OH and 5-/5′-OH. The diprotic origin of EA was convincingly demonstrated by Simić et al.[51] They detected two acidity constants, pK_{a1} and pK_{a2}, with values of 5.42 and 6.76, respectively.

Drug release from nanoparticles depends on several variables, including the type of the polymer, the physicochemical characteristics of the drug, the media's pH, and how the drug interacts with the carrier. The release of EA from the biodegradable nanoparticles occurs through disintegration and diffusion of EA from nanoparticle matrix and finally through degradation of polymer matrix.

The multilamellar structure of CS-NIO-EA NPs exhibited an initial fast release of EA from the surface layer, followed by a diffusion-controlled release from the interior layers. Drugs released through the vesicular system have been noted to have a similar release pattern.[42,52]

The results showed that the encapsulation of EA into CS-NIO-EA NPs produced a slower release profile compared to that of the free EA form because the chitosan coat led to a more controlled release time, which was confirmed by a previous study.[29] The slow release and encapsulation of the drug improved the bioavailability of EA.

2.5. Cell Viability. The cytotoxicity 3-(4,5-dimethylthiazol-2-yl)-2,5-diphenyltetrazolium bromide (MTT) assay results for the different HFB4 cell line treatment samples are shown in Figure 5. UV irradiation reduced cell viability to ∼62%. When EA (20 μg/mL) was added to the UV-exposed cell line sample, the viability was increased up to ∼71.33%, whereas when NIO-EA NPs and CS-NIO-EA NPs (as a treatment formula) were added, the cell viability percentage reached 81.33 and ∼92.66%, respectively. This finding indicates the protective effect of the CS-NIO-EA formulation against UV-induced damage compared with the positive control treated with UV only.

It is evident from these results that the carrier we designed further helped protect the cells due to its permeability properties across cell membranes and its higher drug loading, in addition to the prolonged sustained release. Tween 80 functions as a P-glycoprotein inhibitor. It has been observed that nanoparticles based on Tween 80 can block P-glycoprotein-mediated drug exocytosis.

2.6. Fold Changes in Skin Aging Gene Expression. Figure 6 shows that MMP3 expression increased and Col1A1, Timp3, and TERT expressions decreased in the UV-exposed samples compared to that of the control sample, whereas opposite trends were observed in the UV-EA, UV-NIO-EA, and UV-CS-NIO-EA samples. The best results were observed in the UV-CS-NIO-EA sample, and compared to the UV-exposed sample, MMP3 was reduced by 64.02% and Col1A1, Timp3, and TERT were intensified by 59.24, 83.83, and 63.61%, respectively.

UV-CS-NIO-EA clearly affected the genes responsible for the skin aging process (MMP3, CollA1, and Timp3). It can protect against collagen degradation by downregulating MMP3 expression. Therefore, one strategy to stop UV-induced skin photodamage is MMP3 inhibition. In addition, the upregulation of CollA1 and Timp3 enhances collagen production and inhibits protein degradation in the ECM[20] in human fibroblast cell lines. The intensification of *TERT* protects cells from telomere shortening mediated by oxidative stress induced by UV radiation.

3. CONCLUSIONS

The current findings demonstrate the photoprotective effects of EA on skin wrinkling-induced UV-induced photodamage. The effects were enhanced by the encapsulation of EA in chitosan-coated niosomes, which could represent a good solution for issues associated with degradation and bioavailability. Topical or dietary interventions with EA loaded into chitosan-coated niosomes are promising strategies for alleviating UVA-induced dermal roughening and thickening and thus preventing skin wrinkles and photoaging.

4. EXPERIMENTAL SECTION

4.1. Materials. EA, chitosan (Cs) (low molecular weight, purity ≥ 99%), acetic acid, Tween 80 (purity ≥ 99%), tripolyphosphate, ethanol, and cholesterol (purity ≥ 99.7%, M_W = 386.65) were purchased from Sigma-Aldrich Co. (Schnelldorf, Germany). Phosphate-buffered saline (PBS) with a pH of 7.4 was purchased from Bio Shop Canada Inc. Human fibroblast (HFB4) cells were obtained from Egypt's Vaccines and Sera (VACSERA) Tissue Culture Department. We purchased fetal bovine serum (FBS) from Invitrogen Corp. (Carlsbad, CA). Hank's buffer, trypsin, ethylenediaminetetraacetic acid (EDTA), and penicillin−streptomycin were obtained from Gibco (Grand Island, NY). BioVision, Inc. (Milpitas CA) provided the Qiagen RNA extraction kit, BioRad SYBR green PCR MMX kit, and TERT (Human) ELISA kit. Aktin Chemicals Inc. (Chengdu, China) provided the punicalagin reference standard.

4.2. Methods. *4.2.1. Manufacturing of Niosomes.* Niosomes are formed through a process called thin film hydration.[32,53] Using a 2:1 molar ratio, 10 mL of ethyl alcohol, 10 μL of Tween 80, and 3 mg of cholesterol were poured into a round flask and shaken rapidly until complete dissolution. The thin layers of niosomes were created by evaporating ethanol using a rotary evaporator (Janke & Kunkel RV05-ST, Germany) at 50 rpm, low pressure, and 45 °C. The produced layers were sonicated (WUC-A03H, Daihan, Korea) to produce tiny empty vesicles after hydration with PBS buffer (pH 7.4) containing 2 μg/mL of EA. The capacity of niosomes and chitosan-coated niosomes to encapsulate EA was measured by centrifugation method.[54−56] The sample was centrifuged at 11,000 revolutions per minute at 4 °C for 30 min to remove free EA. The amount of the separated free EA and the total amount of EA were measured spectrophotometrically (JENWAY, 6405 UV/VIS, Barloworld Scientific in Essex, U.K.) by measuring the absorbance of 1 mL of each at 260 nm.[57] The calibration curve of EA was made by plotting the absorbance against concentration. The encapsulation efficiency was calculated using the following equation[32]

$$\text{encapsulation efficiency (\%)} = \frac{\text{total EA} - \text{free EA}}{\text{total EA}} \times 100$$

4.2.2. Preparation of Chitosan-Coated Niosomes. At ambient temperature on a magnetic stirrer, a 25 mL chitosan solution (0.05 g dissolved in 0.01% acetic acid) was mixed with an aqueous solution of niosomes loaded with EA (NIO-EA). Then, 10 mg/mL of triphosphate (10 mL) was added dropwise until a specular suspension of chitosan-coated niosomes loaded with EA (CS-NIO-EA) was formed. The uncoated EA was then removed by centrifuging the mixture at 11,000 rpm and 4 °C for half an hour. The encapsulation efficiency was then calculated.

4.2.3. Characterization of Nanoparticle Formulations. The morphology, size, and surface shape of the nanoparticles were

https://doi.org/10.1021/acsomega.2c07254
ACS Omega 2023, 8, 16620−16629

investigated using TEM (acceleration voltage = 100 kV; JEOL JEM.1230, Japan), DLS, dynamic light scattering (Zetasizer, Malvern Instruments, Malvern, United Kingdom), and SEM (acceleration voltage = 30 kV; field emission model, Quanta 250 FEG).

The created formulations were stained with a 1% aqueous solution of phosphotungstic acid and left to sit for 10 min before being examined via TEM. Using a dynamic light scattering technique, the average size of the nanoparticles distributed in deionized water was determined at 25 °C. For the SEM examination, the samples were lyophilized and capped with platinum.

4.2.4. Ellagic Acid (EA) Release Profile. EA was released using a dialysis procedure.[58] A cellulose acetate dialysis bag (Spectra/P or MW cutoff 12,000, Spectrum, Canada) containing 2 mL of any of the three formulations (free EA, NIO-EA, or CS-NIO-EA) was submerged in 100 mL of PBS buffer. Buffers of different pH values were used for the in vitro drug release studies to simulate the conditions of the stomach (pH 1.2), intestine (pH 6.8), and blood (pH 7.4) and assess the impact of pH on drug release. The mixture was magnetically agitated at 50 rpm. Two milliliters of the release buffer were immediately withdrawn after 1 h. The concentration of EA in the release buffer was measured using a spectrophotometer at 260 nm. The measured release buffer was returned to the mixture. The concentration measurements were repeated 12 times over a 12 h period.

4.2.5. Cell Culture. HFB4 cells were cultured in 75 cm^3 cell culture flasks in Dulbecco's modified Eagle's medium (DMEM) supplemented with 10% FBS, streptomycin (125 μg/mL), penicillin (100 units/mL), sodium pyruvate, and L-glutamate. The cells were incubated in the culture medium at 37 °C for 2 days in a CO_2 incubator (5% CO_2 and 95% relative humidity). The attached cells were collected using trypsin−EDTA (0.05%, Sigma-Aldrich, Germany). After centrifugation with a relative centrifugal force of 210 gravity for 5 min at room temperature, the supernatant was removed, and the cells were resuspended in the exposure medium (DMEM) and counted. The cells were washed with PBS and centrifuged 2 times until reaching at least 80% confluency.[59,60]

4.2.6. UV Irradiation of HFB4 Cells. HFB4 cells were irradiated using a UV-lamp (Bioblock Scientific, Illkirch, France) with a power (P) of 8 W and a wavelength (λ) of 365 nm. A radiometer (VLX-3 W; Cole-Parmer, Vernon Hills, Ill) was used to measure radiant energy. The cells were placed 8 cm from the source and exposed for 1 h. Irradiation was performed in 96-well plates under a laminar flow. After UV irradiation was achieved, the cells were cultured for 24 h at 37 °C, after which the medium was removed via centrifugation. For the upcoming assays, the pellet was resuspended in PBS and then disseminated in tubes of Hank's buffer containing 0.25% of trypsin/EDTA.

4.2.7. MTT (Cytotoxicity) Assay. Cell viability was evaluated using a colorimetric MTT assay. The reduction of the tetrazolium dye MTT to insoluble purple formazan reflects the presence of viable cells. Approximately one million cells were resuspended in 10 mL of the culture medium supplemented with 10% FBS, recultured in 96-microwell plates at a density of $8-10 \times 10^3$ cells per well, and incubated for 1 day at 37 °C. Cell samples were divided into five groups: control; UV (positive control): cell line subjected to UV irradiation (P = 8 W, λ = 365 nm); UV-EA: cell line treated with EA (20 μg/mL) during UV exposure; UV-NIO-EA: cell line treated with NIO-EA NPs during UV exposure; and UV-CS-NIO-EA: cell line treated with CS-NIO-EA NPs during UV exposure. The plates were filtered from the medium and incubated for 24 h at 37 °C before 10 μL of MTT was added to each well. The 96-microwell plates of the five groups were incubated for 4 h at 37 °C, and the plates were measured at 570 nm using an ELISA reader.

4.2.8. Reverse Transcription Polymerase Chain Reaction (RT-PCR) Assay. RT-PCR was performed to measure the fold changes in Col1A1, Timp3, and MMP3 gene expressions, with β-actin used as the housekeeping gene. The RNeasy extraction kit was used to isolate mRNA. Cells were shattered and homogenized using RLT buffer. Ethanol was then added to the mixture to improve the environment for RNA to attach selectively to the RNeasy membrane. The sample was then poured into the RNeasy Mini spin column. Total RNA was linked to the membrane, contaminants were successfully removed, and high-quality RNA was filtered using RNase-free water. Centrifugation was performed in a microcentrifuge to complete the ligation, washing, and rinsing processes. Subsequently, a Master Mix was created, and RT-PCR was used to perform the amplification.

4.2.9. Telomerase Reverse Transcriptase (TERT) Enzyme Assay. A *TERT* (human) ELISA kit (BioVision) was used to prepare reagents, standards, and samples. One hundred microliters of each sample and standard were added to a hygienic plate, which was rinsed twice with a 1× wash solution. The wells were sealed and incubated at 37 °C for 75 min. The contents inside the plate were thrown away without being cleaned or given a chance to properly dry. The wells received 0.1 mL of the biotin-detection antibody work solution before the plate was capped, and incubation was performed for 60 min. After discarding the solution, the plate was cleaned three times by soaking the wells in the buffer solution for a short period of time, decanting the solution, and clapping the plate with absorbent filter papers. The plate was then incubated at 37 °C for 30 min after the addition of the SABC working solution (0.1 mL) to the wells. The solution was removed from the plates and washed five times. After adding 90 μL of TMB substrate, the plate was incubated at 37 °C for 15−30 min in the dark. The procedure was completed by adding 50 μL of stop solution, and the absorbance was read at 450 nm for 20 min.

4.2.10. Statistical Analysis. Data were analyzed using SPSS version 15.0. One-way analysis of variance (ANOVA) was used to determine the differences between groups that were statistically significant at $P < 0.05$. The data are presented as a mean ± SD for three measurements.

AUTHOR INFORMATION

Corresponding Author

Amr A. Abd-Elghany − *Radiology and Medical Imaging Department, College of Applied Medical Sciences, Prince Sattam Bin Abdul-Aziz University, Al-Kharj 11942, KSA; Biophysics Department, Faculty of Science, Cairo University, Giza 12613, Egypt;* orcid.org/0000-0002-7179-2290; Email: amrabdelghany25@gmail.com

Author

Ebtesam A. Mohamad − *Biophysics Department, Faculty of Science, Cairo University, Giza 12613, Egypt*

Complete contact information is available at: https://pubs.acs.org/10.1021/acsomega.2c07254

Notes

The authors declare no competing financial interest.

https://doi.org/10.1021/acsomega.2c07254
ACS Omega 2023, 8, 16620−16629

■ ACKNOWLEDGMENTS

This project was supported by the Deanship of Scientific Research at Prince Sattam bin Abdulaziz University under the research project (PSAU-2022/01/20145).

■ ABBREVIATIONS

UV, ultraviolet; EA, ellagic acid; CS, chitosan; NIOs, niosomes; CS-NIOs, chitosan-coated niosomes; NIO-EA, niosomes loaded by ellagic acid; CS-NIO-EA, chitosan-coated niosomes loaded by ellagic acid

■ REFERENCES

(1) Strnadova, K.; Sandera, V.; Dvorankova, B.; Kodet, O.; Duskova, M.; Smetana, K.; Lacina, L. Skin aging: The dermal perspective. *Clin. Dermatol.* **2019**, *37*, 326−335.
(2) Zouboulis, C. C.; Hoenig, L. J. Skin aging revisited. *Clin. Dermatol.* **2019**, *37*, 293−295.
(3) Łopaciuk, A.; Łoboda, M. In *Global Beauty Industry Trends in the 21st Century*, Management, Knowledge and Learning International Conference, 2013; pp 19−21.
(4) Silverstein, M. J.; Sayre, K. *The Female Economy*; Harvard Business Review, 2009; Vol. *87*, pp 46−53.
(5) Yasin, Z. A.; Ibrahim, F.; Rashid, N. N.; Razif, M. F.; Yusof, R. The importance of some plant extracts as skin anti-aging resources: a review. *Curr. Pharm. Biotechnol.* **2018**, *18*, 864−876.
(6) Menaa, F.; Menaa, A.; Tréton, J. Polyphenols against Skin Aging. In *Polyphenols in Human Health and Disease*; Elsevier, 2014; pp 819−830.
(7) Buranasudja, V.; Rani, D.; Malla, A.; Kobtrakul, K.; Vimolmangkang, S. Insights into antioxidant activities and anti-skin-aging potential of callus extract from Centella asiatica (L.). *Sci. Rep.* **2021**, *11*, No. 13459.
(8) Ray, A.; Gupta, S. D.; Ghosh, S. Evaluation of anti-oxidative activity and UV absorption potential of the extracts of Aloe vera L. gel from different growth periods of plants. *Ind. Crops Prod.* **2013**, *49*, 712−719.
(9) Wang, M.; Charareh, P.; Lei, X.; Zhong, J. L. Autophagy: Multiple mechanisms to protect skin from ultraviolet radiation-driven photo-aging. *Oxid. Med. Cell. Longevity* **2019**, *2019*, No. 8135985.
(10) Mohamad, E. A.; Aly, A. A.; Khalaf, A. A.; Ahmed, M. I.; Kamel, R. M.; Abdelnaby, S. M.; Abdelzaher, Y. H.; Sedrak, M. G.; Mousa, S. A. Evaluation of natural bioactive-derived punicalagin niosomes in skin-aging processes accelerated by oxidant and ultraviolet radiation. *Drug Des., Dev. Ther.* **2021**, *15*, 3151.
(11) Yin, R.; Chen, Q.; Hamblin, M. R. Intense Focused Ultrasound. In *Skin Photoaging*; Morgan & Claypool Publishers, 2015.
(12) Ganceviciene, R.; Liakou, A. I.; Theodoridis, A.; Makrantonaki, E.; Zouboulis, C. C. Skin anti-aging strategies. *Derm.-Endocrinol.* **2012**, *4*, 308−319.
(13) Lephart, E. D. Equol's anti-aging effects protect against environmental assaults by increasing skin antioxidant defense and ECM proteins while decreasing oxidative stress and inflammation. *Cosmetics* **2018**, *5*, 16.
(14) Bae, J. Y.; Choi, J. S.; Kang, S. W.; Lee, Y. J.; Park, J.; Kang, Y. H. Dietary compound ellagic acid alleviates skin wrinkle and inflammation induced by UV-B irradiation. *Exp. Dermatol.* **2010**, *19*, e182−e190.
(15) Gagliano, N.; Arosio, B.; Santambrogio, D.; Balestrieri, M. R.; Padoani, G.; Tagliabue, J.; Masson, S.; Vergani, C.; Annoni, G. Age-dependent expression of fibrosis-related genes and collagen deposition in rat kidney cortex. *J. Gerontol. Ser., A* **2000**, *55*, B365−B372.
(16) Gref, R.; Deloménie, C.; Maksimenko, A.; Gouadon, E.; Percoco, G.; Lati, E.; Desmaële, D.; Zouhiri, F.; Couvreur, P. Vitamin C−squalene bioconjugate promotes epidermal thickening and collagen production in human skin. *Sci. Rep.* **2020**, *10*, No. 16883.
(17) Karsdal, M. *Biochemistry of Collagens, Laminins and Elastin: Structure, Function and Biomarkers*; Academic Press, 2019.
(18) Gutop, E.; Diatlova, A.; Linkova, N.; Orlova, O.; Trofimova, S.; Khavinson, V. Aging of skin fibroblasts: genetic and epigenetic factors. *Adv. Gerontol.* **2019**, *32*, 908−914.
(19) Inanc, S.; Keles, D.; Oktay, G. An improved collagen zymography approach for evaluating the collagenases MMP-1, MMP-8, and MMP-13. *BioTechniques* **2017**, *63*, 174−180.
(20) Lago, J. C.; Puzzi, M. B. The effect of aging in primary human dermal fibroblasts. *PLoS One* **2019**, *14*, No. e0219165.
(21) Buckingham, E. M.; Klingelhutz, A. J. The role of telomeres in the ageing of human skin. *Exp. Dermatol.* **2011**, *20*, 297−302.
(22) Santos, S. A.; Vilela, C.; Domingues, R. M.; Oliveira, C. S.; Villaverde, J. J.; Freire, C. S.; Neto, C. P.; Silvestre, A. J. Secondary metabolites from Eucalyptus grandis wood cultivated in Portugal, Brazil and South Africa. *Ind. Crops Prod.* **2017**, *95*, 357−364.
(23) Bell, C.; Hawthorne, S. Ellagic acid, pomegranate and prostate cancer—a mini review. *J. Pharm. Pharmacol.* **2010**, *60*, 139−144.
(24) El-Sonbaty, S. M.; Moawed, F. S.; Kandil, E. I.; Tamamm, A. Antitumor and antibacterial efficacy of gallium nanoparticles coated by ellagic acid. *Dose-Response* **2022**, *20*, No. 15593258211068998.
(25) Baradaran Rahimi, V.; Ghadiri, M.; Ramezani, M.; Askari, V. R. Antiinflammatory and anti-cancer activities of pomegranate and its constituent, ellagic acid: Evidence from cellular, animal, and clinical studies. *Phytother. Res.* **2020**, *34*, 685−720.
(26) Vilela, C.; Pinto, R. J.; Coelho, J.; Domingues, M. R.; Daina, S.; Sadocco, P.; Santos, S. A.; Freire, C. S. Bioactive chitosan/ellagic acid films with UV-light protection for active food packaging. *Food Hydrocolloids* **2017**, *73*, 120−128.
(27) De, R.; Sarkar, A.; Ghosh, P.; Ganguly, M.; Karmakar, B. C.; Saha, D. R.; Halder, A.; Chowdhury, A.; Mukhopadhyay, A. K. Antimicrobial activity of ellagic acid against Helicobacter pylori isolates from India and during infections in mice. *J. Antimicrob. Chemother.* **2018**, *73*, 1595−1603.
(28) de Souza Tavares, W.; Pena, G. R.; Martin-Pastor, M.; de Sousa, F. F. O. Design and characterization of ellagic acid-loaded zein nanoparticles and their effect on the antioxidant and antibacterial activities. *J. Mol. Liq.* **2021**, *341*, No. 116915.
(29) Kaur, H.; Ghosh, S.; Kumar, P.; Basu, B.; Nagpal, K. Ellagic acid-loaded, tween 80-coated, chitosan nanoparticles as a promising therapeutic approach against breast cancer: In-vitro and in-vivo study. *Life Sci.* **2021**, *284*, No. 119927.
(30) Bala, I.; Bhardwaj, V.; Hariharan, S.; Kumar, M. R. Analytical methods for assay of ellagic acid and its solubility studies. *J. Pharm. Biomed. Anal.* **2006**, *40*, 206−210.
(31) Yasamineh, S.; Yasamineh, P.; Ghafouri Kalajahi, H.; Kalajahi, H. G.; Gholizadeh, O.; Yekanipour, Z.; Afkhami, H.; Eslami, M.; Hossein Kheirkhah, A.; Kheirkhah, A. H.; Taghizadeh, M.; Yazdani, Y. A state-of-the-art review on the recent advances of niosomes as a targeted drug delivery system. *Int. J. Pharm.* **2022**, *624*, No. 121878.
(32) Abd-Elghany, A. A.; Mohamad, E. A. Ex-vivo transdermal delivery of Annona squamosa entrapped in niosomes by electroporation. *J. Radiat. Res. Appl. Sci.* **2020**, *13*, 164−173.
(33) Zhou, X.; Galparsoro, D. F.; Madsen, AØ.; Vetri, V.; van de Weert, M.; Nielsen, H. M.; Foderà, V. Polysorbate 80 controls Morphology, structure and stability of human insulin Amyloid-Like spherulites. *J. Colloid Interface Sci.* **2022**, *606*, 1928−1939.
(34) Abd-Elghany, A. A.; Mohamad, E. A.; El-Sakhawy, M. A.; Mansouri, S.; Ismail, S. H.; Elneklawi, M. S. Enhancement of mechanical properties of chitosan film by doping with sage extract-loaded niosomes. *Mater. Res. Express* **2022**, *9*, No. 035006.
(35) Miatmoko, A.; Safitri, S. A.; Aquila, F.; Cahyani, D. M.; Hariawan, B. S.; Hendrianto, E.; Hendradi, E.; Sari, R. Characterization and distribution of niosomes containing ursolic acid coated with chitosan layer. *Res. Pharm. Sci.* **2021**, *16*, 660.
(36) Kumari, A.; Yadav, S. K.; Yadav, S. C. Biodegradable polymeric nanoparticles based drug delivery systems. *Colloids Surf., B* **2010**, *75*, 1−18.
(37) Abdelbary, G.; El-Gendy, N. Niosome-encapsulated gentamicin for ophthalmic controlled delivery. *AAPS PharmSciTech* **2008**, *9*, 740−747.

https://doi.org/10.1021/acsomega.2c07254
ACS Omega 2023, 8, 16620−16629

(38) Nowroozi, F.; Almasi, A.; Javidi, J.; Haeri, A.; Dadashzadeh, S. Effect of surfactant type, cholesterol content and various downsizing methods on the particle size of niosomes. *Iran. J. Pharm. Res.* **2018**, *17*, 1−11.
(39) Fayed, N. D.; Goda, A. E.; Essa, E. A.; El Maghraby, G. M. Chitosan-encapsulated niosomes for enhanced oral delivery of atorvastatin. *J. Drug Delivery Sci. Technol.* **2021**, *66*, No. 102866.
(40) Caddeo, C.; Díez-Sales, O.; Pons, R.; Carbone, C.; Ennas, G.; Puglisi, G.; Fadda, A. M.; Manconi, M. Cross-linked chitosan/liposome hybrid system for the intestinal delivery of quercetin. *J. Colloid Interface Sci.* **2016**, *461*, 69−78.
(41) Rasul, A.; Khan, M. I.; Rehman, M. U.; Abbas, G.; Aslam, N.; Ahmad, S.; Abbas, K.; Shah, P. A.; Iqbal, M.; Al Subari, A. M. A. In vitro characterization and release studies of combined nonionic surfactant-based vesicles for the prolonged delivery of an immunosuppressant model drug. *Int. J. Nanomed.* **2020**, *15*, 7937.
(42) Arulmozhi, V.; Pandian, K.; Mirunalini, S. Ellagic acid encapsulated chitosan nanoparticles for drug delivery system in human oral cancer cell line (KB). *Colloids Surf., B* **2013**, *110*, 313−320.
(43) Behl, G.; Sharma, M.; Dahiya, S.; Chhikara, A.; Chopra, M. Synthesis, characterization, and evaluation of radical scavenging ability of ellagic acid-loaded nanogels. *J. Nanomater.* **2011**, *2011*, 21.
(44) EL Barky, A. R.; Mohamed, T. M.; Ali, E. M. M. Detoxifying and antioxidant effect of ellagic acid nano particles in rats intoxicated with sodium nitrites. *Appl. Biol. Chem.* **2020**, *63*, No. 47.
(45) Wang, M.; Zhao, T.; Liu, Y.; Wang, Q.; Xing, S.; Li, L.; Wang, L.; Liu, L.; Gao, D. Ursolic acid liposomes with chitosan modification: Promising antitumor drug delivery and efficacy. *Mater. Sci. Eng., C* **2017**, *71*, 1231−1240.
(46) Mohamed AbuElfadl, A.; Boughdady, M.; Meshali, M. New Peceol/Span 60 Niosomes Coated with Chitosan for Candesartan Cilexetil: Perspective Increase in Absolute Bioavailability in Rats. *Int. J. Nanomed.* **2021**, *16*, 5581.
(47) Faheela, M.; Malathi, S. In-vitro characterization of pluronic P 123 based niosome for targeted delivery of doxorubicin. *Mater. Today: Proc.* **2022**, *58*, 795−801.
(48) Shirsand, S.; Para, M.; Nagendrakumar, D.; Kanani, K.; Keerthy, D. Formulation and evaluation of Ketoconazole niosomal gel drug delivery system. *Int. J. Pharm. Invest.* **2012**, *2*, 201−207.
(49) Kamboj, S.; Saini, V.; Bala, S. Formulation and characterization of drug loaded nonionic surfactant vesicles (niosomes) for oral bioavailability enhancement. *Sci. World J.* **2014**, *2014*, No. 959741.
(50) Musialik, M.; Kuzmicz, R.; Pawłowski, T. S.; Litwinienko, G. Acidity of hydroxyl groups: an overlooked influence on antiradical properties of flavonoids. *J. Org. Chem.* **2009**, *74*, 2699−2709.
(51) Simić, A. Z.; Verbić, T. Z.; Sentić, M. N.; Vojić, M. P.; Juranić, I. O.; Manojlović, D. D. Study of ellagic acid electro-oxidation mechanism. *Monatsh. Chem.* **2013**, *144*, 121−128.
(52) Sonaje, K.; Italia, J.; Sharma, G.; Bhardwaj, V.; Tikoo, K.; Kumar, M. R. Development of biodegradable nanoparticles for oral delivery of ellagic acid and evaluation of their antioxidant efficacy against cyclosporine A-induced nephrotoxicity in rats. *Pharm. Res.* **2007**, *24*, 899−908.
(53) Mohamad, E. A.; Mohamed, Z. N.; Hussein, M. A.; Elneklawi, M. S. GANE can Improve Lung Fibrosis by Reducing Inflammation via Promoting p38MAPK/TGF-β1/NF-κB Signaling Pathway Down-regulation. *ACS Omega* **2022**, *7*, 3109−3120.
(54) Bendas, E. R.; Tadros, M. I. Enhanced transdermal delivery of salbutamol sulfate via ethosomes. *AAPS PharmSciTech* **2007**, *8*, 213−220.
(55) Mohamad, E. A.; Aly, A. A.; Khalaf, A. A.; Ahmed, M. I.; Kamel, R. M.; Abdelnaby, S. M.; Abdelzaher, Y. H.; Sedrak, M. G.; Mousa, S. A. Evaluation of natural bioactive-derived punicalagin niosomes in skin-aging processes accelerated by oxidant and ultraviolet radiation. *Drug Des., Dev. Ther.* **2021**, *15*, 3151−3162.
(56) Pham, T. T.; Jaafar-Maalej, C.; Charcosset, C.; Fessi, H. Liposome and niosome preparation using a membrane contactor for scale-up. *Colloids Surf., B* **2012**, *94*, 15−21.
(57) Mohamad, E. A.; Rageh, M. M.; Darwish, M. M. A sunscreen nanoparticles polymer based on prolonged period of protection. *J. Bioact. Compat. Polym.* **2022**, *37*, 17−27.
(58) Henriksen, I.; Sande, S. A.; Smistad, G.; Ågren, T.; Karlsen, J. In vitro evaluation of drug release kinetics from liposomes by fractional dialysis. *Int. J. Pharm.* **1995**, *119*, 231−238.
(59) Badr, D. A.; Amer, M. E.; Abd-Elhay, W. M.; Nasr, M. S.; Abuamara, T. M.; Ali, H.; Mohamed, A. F.; Youssef, M. A.; Awwad, N. S.; Ju, Y.-H.; Fazary, A. E. Histopathological and genetic changes proved the anti-cancer potential of free and nano-capsulated sinapic acid. *Appl. Biol. Chem.* **2019**, *62*, No. 59.
(60) Yang, R.; Zheng, Y.; Li, L.; Liu, S.; Burrows, M.; Wei, Z.; Nace, A.; Herlyn, M.; Cui, R.; Guo, W.; et al. Direct conversion of mouse and human fibroblasts to functional melanocytes by defined factors. *Nat. Commun.* **2014**, *5*, No. 5807.

https://doi.org/10.1021/acsomega.2c07254
ACS Omega 2023, 8, 16620−16629